43rd AIAA Aerospace Sciences Meeting and Exhibit, Jan 10–13, Reno, Nevada

Direct numerical simulation of turbulent jets in crossflow

Suman Muppidi* and Krishnan Mahesh†

University of Minnesota, Minneapolis, MN, 55455, USA

Direct numerical simulations are used to study a round turbulent jet in a laminar crossflow. The velocity ratio of the jet to that of the crossflow is 5.7 and the Reynolds number based on the bulk jet velocity and the jet–exit diameter is 5000. The mean velocity and turbulent intensities from the simulations are compared to data from the experiments by Su & Mungal(2004) and good agreement is observed. A study of the jet cross–section at locations along the jet trajectory explains the differences observed when the trajectories are defined differently – based on the center streamline, the vorticity, and the scalar concentration. The counter–rotating vortex pair is observed all along the length of the jet, though its spatial size is small close to the jet–exit and increases away from it. A recent scaling law for jet trajectory by Muppidi & Mahesh (2005) is used to predict the jet trajectory and shows a reasonable agreement.

I. Introduction

A jet in crossflow is defined as the flow field where a jet of fluid enters and interacts with a crossflowing fluid. Important examples of jets in crossflow are fuel injectors, smokestacks, film cooling on turbine blades and dilution holes in gas turbine combustors. Margason (1993) provides a comprehensive review of the past work on this problem. The emphasis has been on the study of the velocity and vorticity fields (Kamotani & Greber 1972, Fearn & Weston 1974, Andreopoulos & Rodi 1985, Fric & Roshko 1994, Krothapalli *et al.* 1990, Kelso & Smits 1995), study of the scalar field and mixing (Smith & Mungal 1998, Shan & Dimotakis 2000, Su & Mungal 2004) and attempts at modeling the flow field and jet trajectory (Broadwell & Breidenthal 1984, Karagozian 1986, Hasselbrink & Mungal 2001, Muppidi & Mahesh 2005).

Some of the recent work on jets in crossflow involves numerical simulations. Chochua *et al.* (2000) performed RANS calculations and compared their results to experiments (UTRC). It was seen that though their simulations predicted the mean velocities reasonably, their turbulent intensities showed significant differences from those of the experiment. Yuan *et al.*(1999) performed LES of a round jet in crossflow and showed reasonable agreement for mean velocities and turbulent intensities with experimental results of Sherif & Pletcher (1989). Schluter & Schonfeld (2000) compared the results of their LES with experimental velocity profiles of Andreopoulos & Rodi (1984) and scalar fields of Smith & Mungal (1998), and obtain reasonable agreement with the experiments.

The objective of this paper is to study the features of a round turbulent jet in crossflow using direct numerical simulations. The simulations are performed at conditions corresponding to the experiment by Su & Mungal (2004). This paper is organized as follows. Section II describes the problem and the relevant parameters. Section III provides the details of the simulations. Results are provided in section IV: the comparison with Su & Mungal's (2004) experiments are presented in subsection A and the velocity field in the near–field is discussed in subsection B. The evolution of the jet as it moves away from the jet–exit is studied in subsection C and a method to predict jet trajectories is presented in subsection D. The paper ends with a short summary in section V.

*Graduate Research Assistant

†Assistant Professor

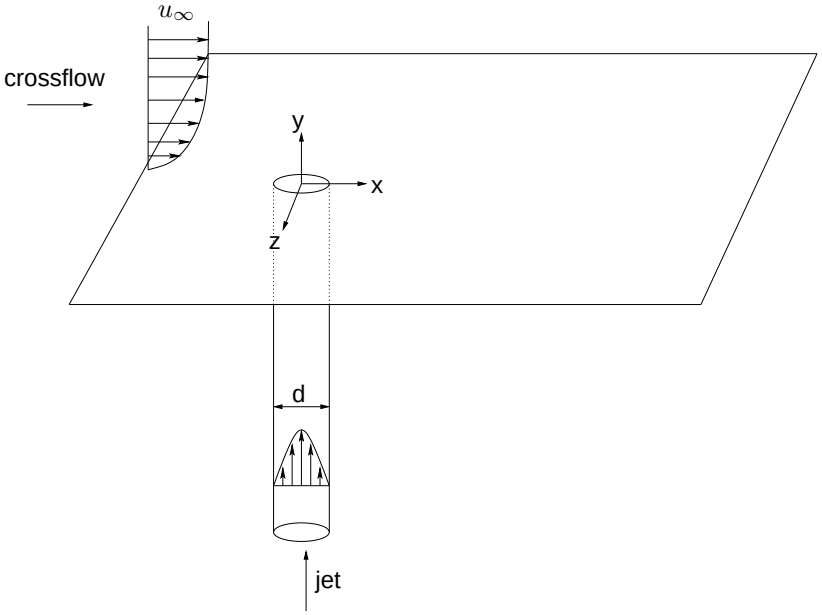

Figure 1. Schematic of the problem.

II. Problem

Figure 1 shows a schematic of the problem, where a jet issues perpendicularly from a round pipe into the crossflow. The crossflow is in the x–direction and the jet is in the y–direction. The origin is located at the center of the jet exit as shown. u_∞ is the crossflow free stream velocity. The velocity ratio is defined as $r = \overline{u}_j/u_\infty$, where $\overline{u}_j$ is the mean jet velocity obtained by averaging u_j over the pipe cross–section.

Simulations are performed under the conditions pertaining to experiments by Su & Mungal (2004). The velocity ratio (r), defined as above, is 5.7 and the Reynolds number of the flow, based on the bulk jet velocity and the jet–exit diameter is 5000. In the experiment, the jet exits out of a round pipe (of length, about 70 d) into the crossflow. In the absence of any crossflow, fully developed pipe flow conditions are expected at the jet–exit (Su & Mungal, section 2). Their experiment considered two cases – one where the jet–exit was flush with the wall and another where the pipe protruded into the crossflow and away from the flow boundaries. The simulations are confined to the case of the jet–exit flush with the wall of the crossflow, as seen in figure 1. The crossflow is laminar and the 80% boundary layer thickness is $\delta_{80\%} = 1.32d$ at the location of the center of the jet–exit, and in the absence of the jet.

III. Simulation details

A. Algorithm

The numerical scheme solves the incompressible Navier Stokes equations

$$\frac{\partial u_i}{\partial t} + \frac{\partial u_i u_j}{\partial x_j} = -\frac{\partial p}{\partial x_i} + \nu \frac{\partial^2 u_i}{\partial x_j x_j} \ , \quad \frac{\partial u_i}{\partial x_i} = 0 \tag{1}$$

on unstructured grids. Here u_i, p and ν denote the velocities, pressure and kinematic viscosity respectively. The density of the fluid is assumed constant and is absorbed into the pressure. The numerical scheme has been described by Mahesh *et al.* (2004) and will not be dealt with here in detail. The algorithm stores the Cartesian velocities and the pressure at the centroids of the cells (control volumes) and the face normal velocities are stored independently at the centroids of the faces. The scheme is a predictor–corrector formulation which emphasizes discrete energy conservation on unstructured grids. This property makes the algorithm robust at high Reynolds numbers without numerical dissipation. The predicted velocities at the control volume centroids are obtained using the viscous and the non–linear terms of equation 1 which are then used to predict the face normal velocities

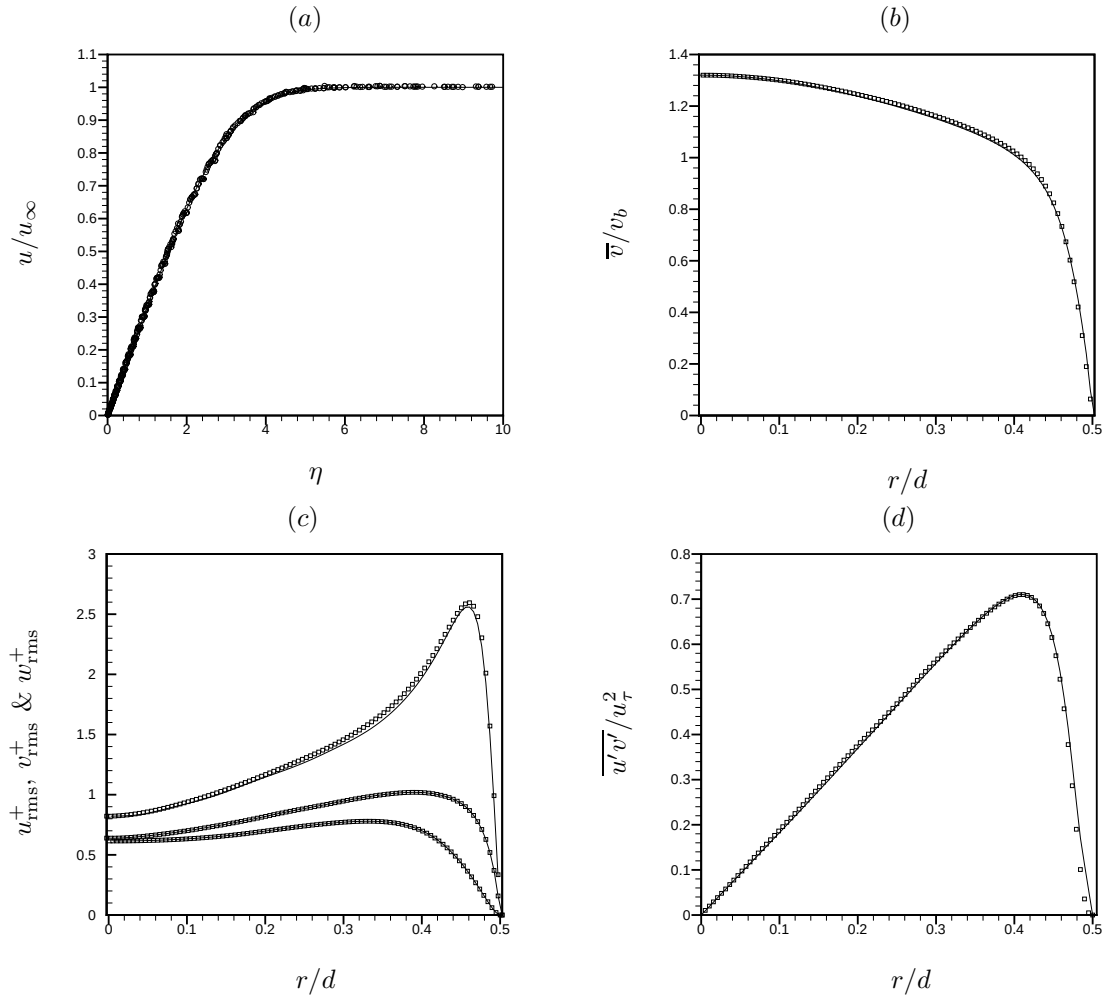

Figure 2. (*a*) **Validation of the crossflow. Comparison with analytical Blasius solution.** ○ **: simulations,** ——— **: Analytical solution.** (*b*)**,** (*c*)**&** (*d*) **Validation of the turbulent pipe flow. Comparison to data from Eggels** *et al.* **(1994).** ——— **: simulation,** □ **: Eggels** *et al.*

on the faces. The predicted face normal velocity is projected so that continuity is discretely satisfied. This yields a Poisson equation for pressure which is solved iteratively using a multigrid approach. The pressure field is used to update the Cartesian control volume velocities. Implicit time–stepping is performed using a Crank–Nicholson scheme. The algorithm has been validated for a variety of problems (see Mahesh *et al.* 2004) over a range of Reynolds numbers.

B. Computational Domain and Boundary Conditions

The computational domain extends $32d \times 64d \times 64d$ in the axial, wall-normal and spanwise directions (x, y and z) respectively. Preliminary computations showed that a domain of this size does not constrain the jet, and the flow does not feel the effects of confinement by the boundary. A length of pipe $2d$ is included in the computational domain in order to allow the fully developed turbulent pipe flowfield (at the inlet) to adjust to the interaction between the jet and the crossflow. The crossflow inflow plane is located $4d$ upstream of the jet–exit.

The crossflow is modeled as a laminar flow past a flat plate (Schlichting 1968). In the absence of the jet, the crossflow has a boundary layer thickness of $\delta_{80\%} = 1.32d$ at the center of the jet–exit. At the crossflow inflow plane, the velocity field is specified, based on the analytical solution to the Blasius boundary layer, to give the required δ at the jet–exit in the absence of the jet. In order to validate the crossflow, a simulation of only the crossflow is performed on a domain without the pipe. The mesh used for the the validation was

considerably coarser than the one used in the jet in crossflow DNS: the mesh edgelengths in the streamwise and the spanwise directions were 5–10 times the corresponding ones in the current DNS. Figure 2(a) shows the results of this validation. Streamwise velocity u is plotted, at all the points of the domain, as a function of the similarity variable η. The symbols show the results from the simulation and are compared to the analytical Blasius solution (shown in a solid line) for laminar flow past a flat plate. Note that the comparison shows a good agreement.

The jet in the experiment is turbulent and fully developed by the time the fluid exits the jet–exit. In order to simulate such a jet, a separate computation is performed to simulate fully developed turbulent flow in a pipe. This computation is performed at a Reynolds number, based on the pipe diameter and the mean axial velocity, of 5000. Figures 2(b), (c) & (d) show the validation of the results of this simulation by comparing the radial profiles of velocity and intensity to the results of Eggels *et al.* (1994). Mean axial velocity $\overline{v}$ is normalized with the bulk velocity v_b (figure 2(b)). The rms velocities in figure 2(c) are normalized with the friction velocity u_τ, and the Reynolds shear stress in figure 2(d) is normalized by the shear stress at the wall. The profiles shown in solid lines are from the present simulation and the square symbols denote the results of Eggels *et al.* (1994). Note that a good agreement is obtained. The mesh used to compute the pipe flow is structured, and contained $256 \times 96 \times 128$ points in the axial, radial and the azimuthal directions respectively. In terms of wall units, the grid spacing is $\Delta x^+ = 6.762$, $\Delta r^+ = 1.802$, and in the azimuthal direction, the minimum and maximum spacings are $\Delta\theta^+ = 0.0042$ and 8.447 respectively. A time–dependent velocity field at a cross–section plane from the pipe flow simulation is fed at the inflow plane of the pipe, as the boundary condition for the jet. In order to do this, once the solution for the pipe flow simulation achieves a steady mean discharge, the instantaneous velocity field (at the plane) over 80 time units (d/u_∞) is stored. The boundary condition specification also involves an amount of interpolation since the computational mesh on the cross–section plane of the turbulent pipe simulations is different from the mesh on the inflow plane of the pipe in the jet in crossflow simulation. More details about the mesh used on the inflow plane are provided in subsection C.

On the exit plane ($x/d = 32$), a zero–gradient boundary condition is used for the velocities. On the spanwise boundaries ($z/d = \pm\ 32$), the velocity field corresponding to the laminar crossflow is specified. Freestream velocity boundary condition is specified on the top boundary ($y/d = 64$).

C. Computational Mesh

The computational mesh is unstructured and consists of approximately 11 million hexahedral elements. The finest elements are found at the walls of the pipe and of the crossflow. The largest elements are found away from the jet–exit and away from the wall. The mesh is constructed as follows. The inflow plane for the pipe (y/d = –2) is first meshed. 128 elements are used in the azimuthal direction and 72 elements in the radial direction (up to a depth of about $0.4d$ inwards from the wall). This part of the face mesh is structured. The rest of the plane is meshed using unstructured elements of size (edge length) $0.005d$. This face mesh is now swept in the y–direction up until the jet–exit ($y/d = 0$). The mesh size in this direction is $0.02d$. Note that the mesh in this part of the domain is based on the mesh used to simulate the turbulent pipe flow specified at the inlet. The wall of the crossflow is then meshed. The size of the mesh elements in the region around the jet–exit is allowed to grow (with 128 azimuthal elements) linearly outward at a ratio of 1.05. This is done till the elements grow to a size of $0.1d$. The region of interest, roughly spanning $5d$ either side of the symmetry plane and up to $20d$ downstream of the jet–exit, is meshed using unstructured elements of size 0.1–$0.15d$. The rest of the plane is then meshed with elements that are allowed to grow large, away from the region of interest. Mesh elements of around $1.0d$ are found at distances about $24d$ away from the symmetry plane and around $24d$ downstream of the jet–exit. The mesh size variation is not allowed to be unreasonably high anywhere in or near the region of interest. The mesh on the plane $y/d = 0$ is now swept in the y–direction. A boundary layer at the crossflow wall allows fine elements near the wall ($\Delta y = 0.01d$) and the mesh size increases linearly away from it at a rate of 1.05 till the mesh size is $0.1d$. Δy is kept constant until a height of $y/d = 24$. Past this plane (note that jet exits the domain before crossing this plane), Δy is allowed to grow linearly at a rate of 1.1. Figure 3(a) provides a horizontal slice of the mesh. The fine elements in and around the jet–exit and in the vicinity of the symmetry plane are noticeable. Since the mesh on the wall is swept in the vertical (y–axis) direction, a horizontal section at any height above the jet–exit shows the same computational mesh as figure 3(a). Note that the complete domain is not shown.

The details provided above (for the computational domain, mesh and the boundary conditions) are arrived at, after a series of simulations at different computational parameters. For example, the simulation was performed

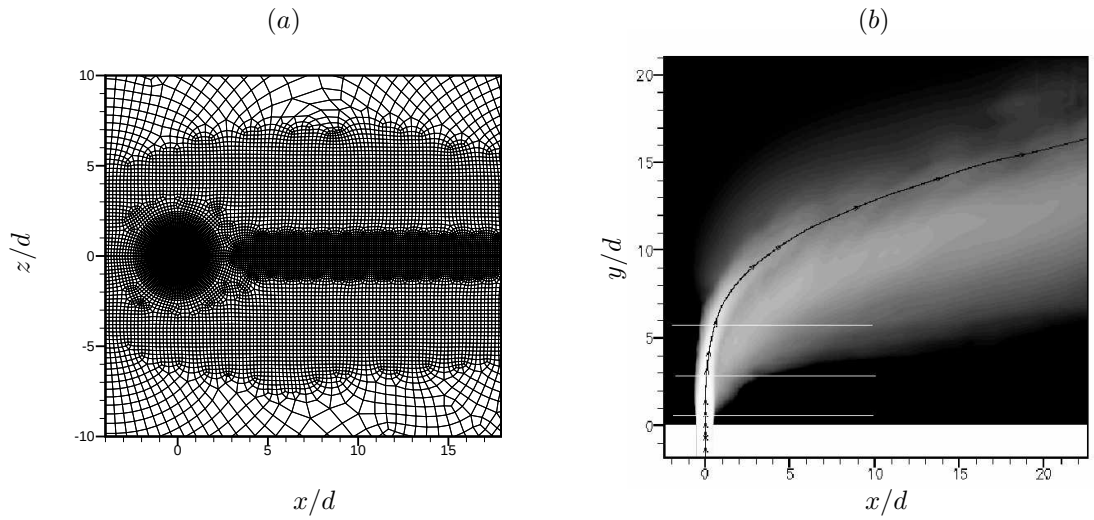

Figure 3. (a) **Horizontal slice of the computational mesh shows the elements in the region around the jet–exit and on the symmetry plane where the profiles are compared. Shown is only a part of the domain.** (b) **Time–averaged contours of velocity (v) on the symmetry plane. Also shown is a mean streamline. The white horizontal lines show the stations at which the computational results are measured with that of the experiment (section IV subsection A).**

on domain sizes extending, in the x, y and z–directions respectively, $32d \times 32d \times 12d$ and $32d \times 64d \times 12d$ before the present simulation where the domain is $32d \times 64d \times 64d$, and which does not restrict/confine the jet. The computational mesh used in the preliminary simulations contained 2.4 million elements, which was refined to a mesh containing about 6 million elements and, later, 8 million elements, and the present mesh contains about 11 million elements. Particular care was taken to prescribe the boundary conditions for the simulation and especially for the jet at the jet inflow which is $2d$ upstream of the jet–exit. The preliminary simulations have shown that this length of pipe is sufficient, at this velocity ratio, to let the jet develop naturally before issuing into the crossflow. Such a conclusion was reached after using a pipe of length $10d$ and observing the velocity profile of the fluid inside the pipe between the jet inflow plane and the jet–exit. As explained in section B the jet inflow boundary conditions are prescribed that match validated results for a fully turbulent flow in a pipe, and the computational mesh in the near–field of the jet–exit is determined based on the computational mesh used in the turbulent pipe flow simulation.

IV. Results

The simulation was performed at a time step of 0.0025 non–dimensional time units (d/u_∞). The computation is begun with a 'no–flow' initial condition. The solution is allowed to evolve until about 80 time units by which time the transients exit the computational domain. Statistics are then computed over 40 time units.

Contours of time–averaged velocity (v) on the symmetry plane are shown in figure 3(b). The jet fluid decelerates, away from the jet–exit as observed in the figure. Also shown is a mean centerline streamline, representing the path taken by the jet fluid as it interacts with the crossflow. Note that the jet is not symmetric about the mean streamline. The jet appears thinner on the upstream side of the streamline and thicker on the downstream side. This aspect is further discussed in subsection B.

A. Comparison to experiments

Note that figure 3(b) shows three horizontal lines on the symmetry plane corresponding to distances, from the wall, of $0.1rd$, $0.5rd$ and $1.0rd$. Su & Mungal (2004) provide detailed experimental profiles of velocity and turbulent intensities at these stations, as a function of the non–dimensionalized streamwise distance (x/rd). Figure 4 shows profiles of $\overline{v}$, $\overline{v'v'}$, $\overline{u'u'}$ and $\overline{u'v'}$ from the simulation and are compared to the experimental results. The solid lines in these plots are results from the present simulation while the symbols are the results

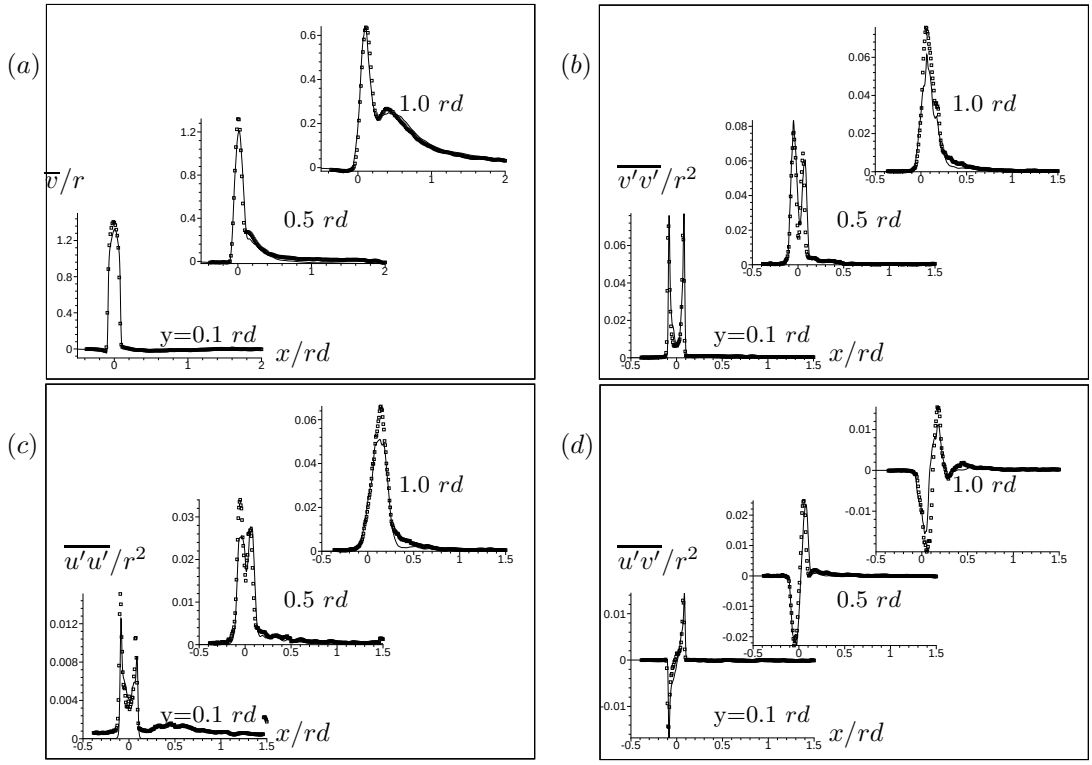

Figure 4. Comparison of mean vertical velocity ($\overline{v}$) and turbulent intensity ($\overline{v'v'}$, $\overline{u'u'}$ and $\overline{u'v'}$) profiles with the experimental results. ——— Simulation, ◻ experiment. Profiles are at stations y = 0.1 rd, 0.5 rd and 1.0 rd.

from the experiment.

Plots of $\overline{v}$, in figure 4(a), show that the peak vertical velocity is observed near the center of the jet–exit at the closest station. Moving away from the wall, the location of peak $\overline{v}$ is observed downstream of the jet–exit. This can be explained in terms of the jet trajectory, the jet bending in the direction of the crossflow. Also, the value of the peak velocity decreases away from the wall as can be observed. Figure 4(b) shows profiles of $\overline{v'v'}$. At $y/rd = 0.1$, $\overline{v'v'}$ shows two peaks corresponding to the edges of the jet, at locations indicated by the leading and the trailing edges of the jet–exit ($x/d = \pm\ 0.5$). The two peaks appear to have the same value. At the second station ($y/rd = 0.5$), the plot still shows two peaks, however, with different peak values. The upstream edge of the jet shows a higher $\overline{v'v'}$ than the downstream edge of the jet, suggesting a higher shear rate on the upstream edge. The farthest station shows a single peak. It may be noticed that the peak $\overline{v'v'}$ at the three stations is of the same order and that no significant change in the peak value is observed moving away from the wall. Profiles of $\overline{u'u'}$ (figure 4(c)) also show a twin–peak close to the wall and a single–peak at the station farthest from the wall. In addition, the peak $\overline{u'u'}$ is observed to increase with the distance from the wall. Figure 4(d) shows the profiles of $\overline{u'v'}$ and it is seen that the profile changes sign between the peaks. The peak $\overline{u'v'}$ value increases in magnitude from $y/rd = 0.1$ to $y/rd = 0.5$ and decreases by $y/rd = 1.0$. Note that the magnitude of the peak $\overline{u'v'}$ is slightly higher on the upstream edge of the jet than on the downstream edge. The profiles also suggest that the width of the peaks increases moving away from the jet–exit. This is observed by noting that the gradient of the profile (around the peak) at the closest station seems sharper than that seen at the other two stations. It should be mentioned that all the profiles (as observed in the $\overline{v}$ profiles) show a shift of the location of the peak in the downstream direction, away from the wall.

Though figure 4 shows a reasonable agreement between the simulation and the experiment, a few discrepancies can be noticed. The peak vertical velocity $\overline{v}$ (figure 4(a)) from the experiment is higher than that observed in the simulations, particularly at the first two stations. Similar differences can be seen with regards to the peaks while comparing $\overline{u'u'}$ in figure 4(c), and $\overline{u'v'}$ in figure 4(d). While the $\overline{v}$ profile shows the greatest discrepancy at the location closest to the jet–exit, the profiles for $\overline{u'u'}$ and $\overline{u'v'}$ show the greatest difference at the location

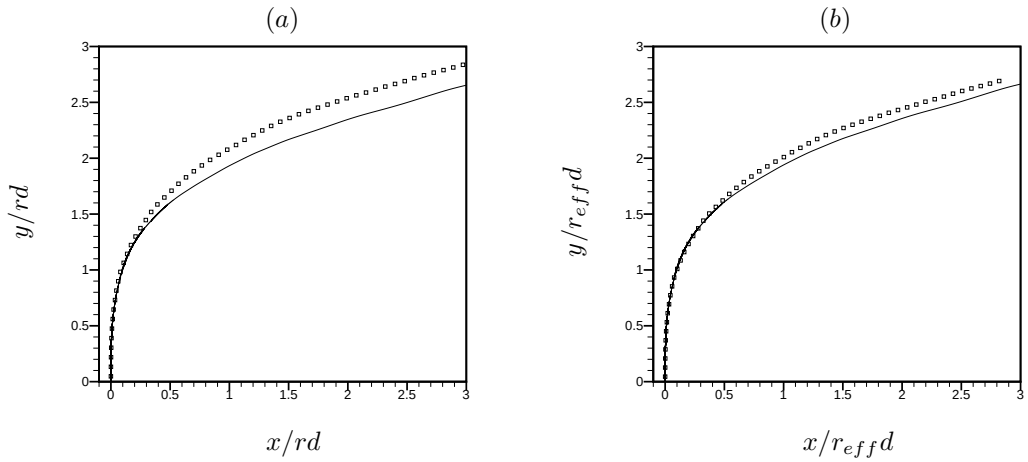

Figure 5. Comparison of jet trajectory from the simulation (———) to that from the experiment (□). (a) scaled using r, and (b) scaled using r_{eff}.

farthest from the jet–exit. Attempts to explain these differences follow.

Su & Mungal report that the bulk jet velocity ($\overline{u_j}$) in their experiment is 16.9 m/s and that the freestream crossflow velocity (u_∞) is 2.95 m/s, which gives a velocity ratio ($r = \overline{u_j}/u_\infty$) of 5.7. The velocity ratio in the simulations, is also 5.7 based on the bulk jet velocity and the freestream crossflow velocity. The Reynolds number, based on the bulk jet velocity and the jet–exit diameter, is 5000 and matches that in the experiment. Yet, as mentioned above, a few differences are seen comparing the experimental results with that of the simulation.

One possible reason for the differences could be the difference in densities. The simulation assumes both the jet fluid and the crossflow fluid to have the same density. In the experiment, the jet fluid (nitrogen) is seeded with acetone vapor which gives the jet fluid, a 10 % higher density ($\rho_j/\rho_\infty = 1.1$, Su & Mungal 2004). If the velocity ratio (r_{eff}) were to be defined based on the momentum :

$$r_{eff}{}^2 = \frac{\rho_j \overline{u_j}^2}{\rho_\infty {u_\infty}^2} = \frac{\rho_j}{\rho_\infty} r^2, \tag{2}$$

the flow parameters described in Su & Mungal (2004) provide a $r_{eff} = 6.008$. As a jet of fluid with a density 10% higher than that of the crossflow exits the jet–exit, it has a momentum that is 10% higher than a jet with the same fluid density as that of the crossflow fluid. This higher momentum could lead to higher peak velocities ($\overline{v}$), sharper intensity gradients and a trajectory that penetrates deeper into the crossflow. It has been previously noted (Muppidi & Mahesh 2005) that the flow field of a jet in crossflow is very sensitive to the jet inflow at the jet–exit. This 10% momentum difference, hence, could be responsible for the discrepancies observed. The differences seen in figure 4 seem consistent with the above explanation. Figure 5(a) compares the experimentally observed jet trajectory to the trajectory extracted from the simulations. As predicted above, the jet in the experiment penetrates deeper into the crossflow (as a result of having a higher momentum). It should be mentioned here that the jet trajectory from the experiment is extracted using the local scalar maxima, and the trajectory from the present computation is defined based on the streamline passing through the jet–exit on the symmetry plane. It has been shown (Su & Mungal 2004, figure 19) that the trajectory defined based on the center streamline penetrates deeper into the crossflow than the trajectory that is defined based on the local scalar maxima. Figure 5(a) shows, however, that due to the difference in the densities, the trajectory based on the center streamline penetrates less than the scalar maxima trajectory from the experiment.

A reasonable approach to compare the experimental and computed results is to use r_{eff} to scale the results instead of r. Such a scaling would account for the density ratio of the jet and the crossflow fluids. Jet trajectories scaled using r_{eff} are shown in figure 5(b). $r_{eff} = 5.7$ for the simulation and $r_{eff} = 6.008$ for the experiment, a difference of about 6.7 %. It is observed that rescaling the trajectories brings them considerable closer to each other. At an x location $15d$ downstream of the jet–exit, the difference between the trajectories scaled with rd is about 6.5 % while scaling the trajectories using $r_{eff}d$ reduces the difference to 2.8%.

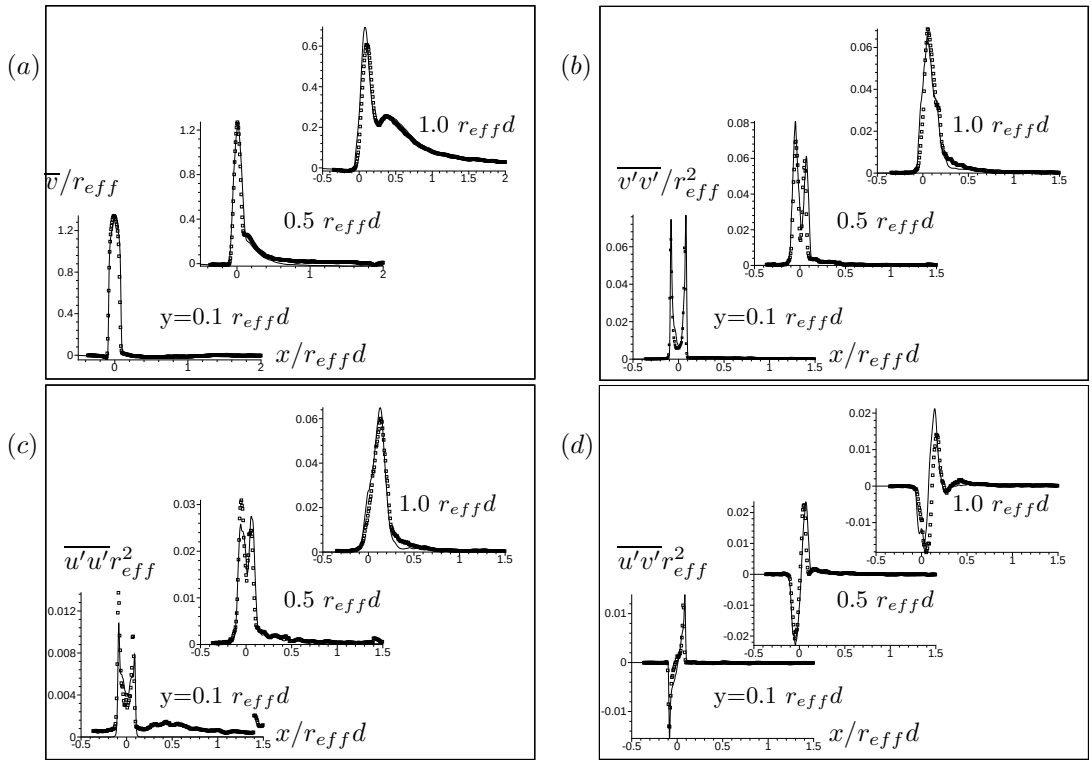

Figure 6. Comparison of mean vertical velocity ($\overline{v}$) and turbulent intensity ($\overline{v'v'}$, $\overline{u'u'}$ and $\overline{u'v'}$) profiles with the experimental results. ——— simulation, ▫ experiment. Plots normalized using r_{eff}.

The velocity and intensity profiles (figure 4) can be similarly re-scaled using r_{eff} and these profiles are shown in figure 6. As earlier, the lines show results from the simulations and the symbols show results from the experiment. The profiles correspond to the locations $y/r_{eff}d = 0.1$, 0.5 and 1.0, and the mean velocity and the intensities are scaled with r_{eff}. The velocity ($\overline{v}$) profiles in figure 6(a) show a good agreement, even for the peak $\overline{v}$ values at the first two locations (as compared to figure 4(a)). The peak velocity on the farthest station ($y/r_{eff}d$ = 1.0), however, shows a slight difference. The profile from the simulation is observed to be higher than that obtained from the experiment. Profiles of $\overline{v'v'}$ (figure 6(b)) also show a good agreement with the experiment at all the three y/r_{eff} locations. Comparison of profiles of $\overline{u'u'}$ ((figure 6(c)) show a slight difference in the peak values at the leading edge of the jet at the first two locations. Good agreement is obtained at $y/r_{eff} = 1.0d$. Note that this profile, when scaled using r, in figure 4(c) showed the most difference between the simulation and the experiment. Figure 6(d) shows a comparison of $\overline{u'v'}$. At the first two stations, a very good agreement is observed, while the profiles at the farthest station show a difference. The experimental peaks appear to occur slightly more downstream of the jet–exit than seen in the profiles obtained from the computation. Overall, for all the quantities compared and at all the locations, the agreement presented is quite reasonable, particularly, when seen in the context of the sharp gradients that the profiles possess (*e.g.* $\overline{v'v'}$ and $\overline{u'v'}$ at $y/r_{eff}d = 0.1$).

The comparisons shown above (figures 4, 5 and 6) can be summarized as follows :

- Velocity and intensity profiles show significant differences when plotted on axes scaled using r. Experimental velocity and intensity peaks are higher than those computed. This suggests that the velocity ratio r does not completely scale the flow field.
- Jet trajectories,plotted on axes scaled with rd show the experimental trajectory to penetrate deeper into the crossflow than that from the simulation. When plotted on axes scaled using $r_{eff}d$, the trajectories show a better collapse.
- Re-scaling the profiles with r_{eff} brings the profiles significantly closer. This suggests that a velocity ratio r_{eff} based on the momentum (and which accounts for the density ratio) is more applicable than r to scale

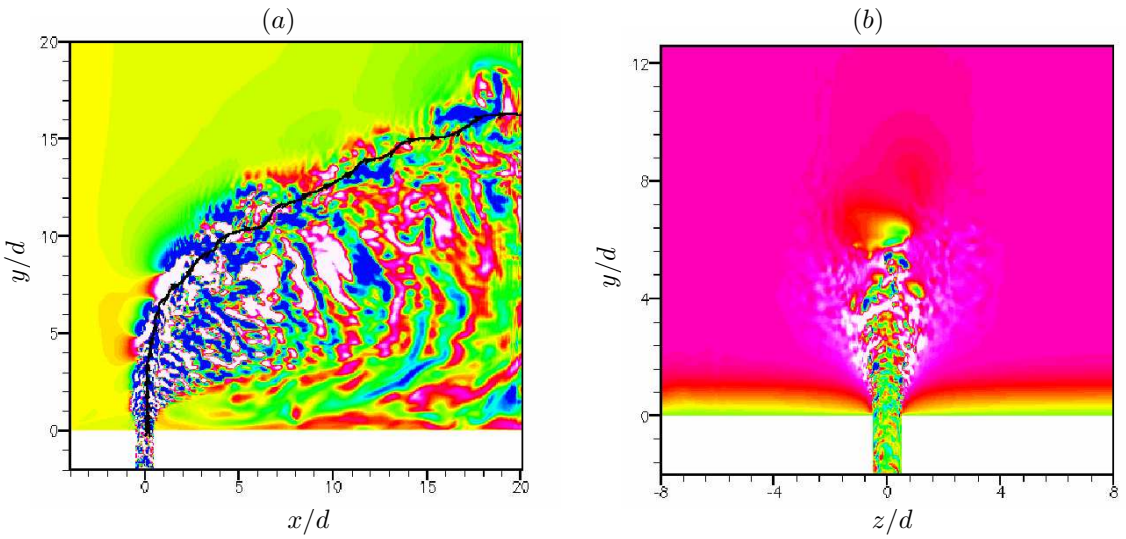

Figure 7. (a)Instantaneous contours of spanwise velocity (w) on the symmetry plane. (b)Instantaneous contours of velocity (u) on the end-on plane ($x/d = 0$).

the flow field.

B. Velocity Field

Figure 7(a) shows the instantaneous contours of spanwise velocity (w) on the symmetry plane. Note the small scales of motion seen inside the pipe and close to the jet–exit. Note that the crossflow fluid upstream of and above the jet shows zero spanwise velocity (w) and that the crossflow fluid downstream of the jet–exit shows a small velocity. The extent of the jet on the symmetry plane is, thus, well represented by these contours and provide an idea of the jet–width on the symmetry plane. Also shown is an instantaneous streamline on the symmetry plane passing through the center of the jet–exit. It may be observed that the jet is wider downstream of this streamline (positive x side of the centerline) as compared to the upstream side. This asymmetry has been noted by Su & Mungal (2004, figure 8) and they cite the reason to be due to the 'jet fluid that is stripped away from the developing region of the jet by the crossflow and is deposited in the wake region'. This suggests that the jet fluid seen downstream of the streamline exits the jet–exit lying on the periphery (of the jet) and not on the symmetry plane. Also note that the crossflow fluid has a higher momentum upstream side of the jet (negative x side of the jet centerline) as compared to the downstream side (the 'wake' region) of the jet. This difference in momentum could also aid in accentuating the above seen asymmetry in the jet width. Such an asymmetry is also observed in figure 3(b) where the time–averaged velocity contours are shown. Instantaneous contours of the streamwise velocity (u) on the end–on plane ($x/d = 0$) are shown on figure 7(b). The direction of the crossflow fluid, in this figure, is into the plane of the paper. Small scale flow features are clearly seen inside the pipe and near the jet–exit as the jet fluid exits into the crossflow. The three–dimensionality of the flow field is also apparent. Outside this interaction region (past about 5 to 8 diameters away from the jet–exit), the crossflow fluid appears relatively quiescent. The contours show the crossflow boundary layer thickness to reduce, close to the jet–exit. This is due to the acceleration of the crossflow fluid as it flows past (around) the jet.

As mentioned earlier, the inflow condition at the pipe entrance is a time–dependent velocity field from the computation of a fully developed turbulent flow in a pipe. The length of pipe included in the domain allows the jet to develop naturally prior to exiting into the crossflow. Figure 8(a) shows the velocity ($\overline{v}$) profiles on the symmetry plane across the pipe diameter at different stations parallel to the wall (x–z plane). Shown are the profiles at y/d = –2, –1, 0, 1, 2, and 3. Note that the first three profiles shown (y/d = –2, –1 and 0) do not differ much from each other. This would suggest that the length of pipe used in the computations is sufficient to model the problem. The differences, though small, between the profile at the pipe inlet and the profile at the jet–exit, suggest the necessity of including some length of pipe in the computational domain. This aspect has been earlier mentioned by Yuan & Street (1999) and Muppidi & Mahesh (2005). The profiles in figure 8(a) show that moving away from the jet–exit, as might be expected, the peak velocity decreases and the peak shifts to

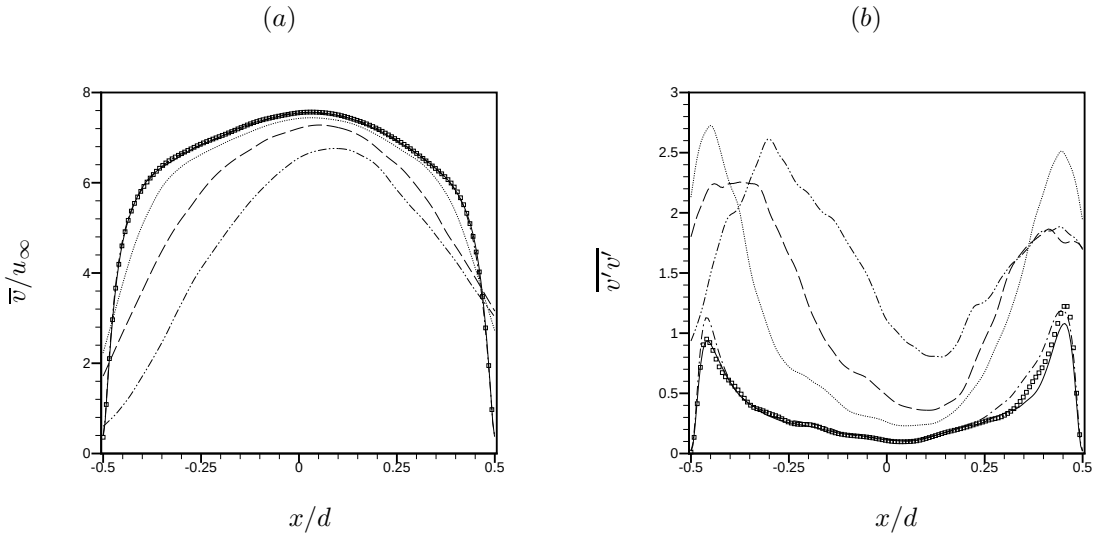

Figure 8. Profiles of velocity(v) and turbulent intensity ($\overline{v'v'}$) across the jet diameter at different stations parallel to the wall : ——— $y/d = -2$, □ -1, —·— 0, ····· 1, – – – 2 and —··— 3.

the right. The jet decelerates as it interacts with the crossflow, and the momentum of the crossflow forces the jet to move to the right, hence shifting the location of the peak velocity. profiles of turbulent intensity ($\overline{v'v'}$) are presented in figure 8(b). At the inflow of the pipe, the profile shows two peaks of almost equal value and is symmetric about the origin. As the jet fluid gets closer to the jet–exit, the profile begins to lose the symmetry. Both the peaks are shifted to the right, and the peak on the right side (downstream edge) has a value higher than that of the peak on the left side (upstream edge) of the origin. Once the fluid exits the jet and interacts with the crossflow, there is a significant increase in the turbulent intensity as is clearly seen. Also noticeable is the shift of the locations of the peak intensity in the direction of the crossflow.

C. Evolution of the jet

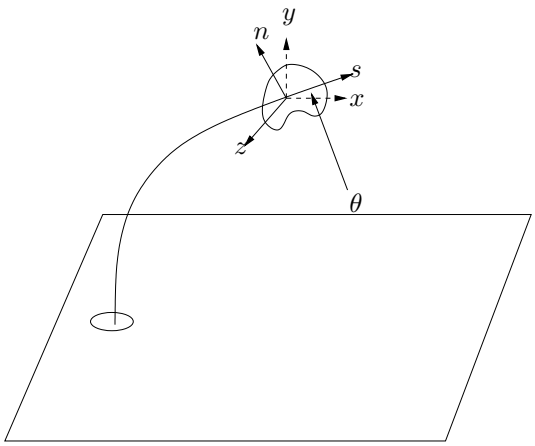

Figure 9. Schematic of the axes used to show the evolution of the jet along the trajectory. θ is the angle by which the x–y axes are rotated about the z–axis to obtain the s–n axes system.

It is well known that as a jet issues into the crossflow, not only does it deflect in the direction of the crossflow, but also forms a pair of counter–rotating vortices. The counter–rotating vortex pair (CVP) has been considered to be a dominant feature of this flow and has been observed to persist far downstream (Keffer & Baines 1963, Pratte & Baines 1967, Kelso *et al.* 1996). It is convenient to study the evolution of the jet in a coordinate system that is aligned with the jet. A schematic of this coordinate system is presented in figure 9. At any point along the centerline of the jet (defined by the mean jet trajectory) a new coordinate system s–n is obtained by rotating

the x–y axes about the z–axis. The angle of rotation is θ. Very close to the jet–exit, $\theta \sim 90°$. In the far–field, when the jet is horizontal, $\theta \sim 0$ and the s–n axes are the same as the x–y axes. The z–coordinate is the same in both the coordinate systems. On the s–n plane, note that s is the coordinate along the jet centerline, and n is the coordinate normal to the centerline. By a simple coordinate transformation, the velocity field can be expressed in terms of u_s, u_n and w, along the s,n,z–axes. Figure 11 shows the jet on planes perpendicular to the jet at different s locations. The in–plane coordinates are z and n. Shown are the contours of out–of–plane velocity (u_s) along with a few in–plane streamlines. The origin on these planes indicates the location where the jet centerline crosses the plane. The plots are at locations $s = d$, $4d$, $7d$, $10d$, $13d$ and $15d$. At these locations, θ is, respectively, 89.75°, 81.44°, 62.26°, 40.71°, 30.3° and 24.49°.

The cross–section of the jet changes along the jet trajectory. Close to the jet–exit ($s = d$, figure 11a), the jet has a circular cross–section, and the highest velocity is seen in the middle of the jet cross–section, around the centerline. Away from the jet–exit, the jet cross–section begins to flatten at the trailing edge (figures 11b and c) giving the jet a 'kidney–shaped' structure, and even further away (figures 11d–f), velocity contours show the trailing edge to move closer to the leading edge. The higher velocity contours, away from the jet–exit, are seen on the edges of the jet cross–section and the fluid in the middle appears to have a relatively lower velocity.

At $s = d$, streamlines show a significant entrainment of the crossflow fluid by the jet. This entrainment appears to influence (entrain) crossflow fluid that is as far as $3d$ away from the jet center. At the trailing edge of the jet, the streamlines show the presence of a vortex pair, restricted to a small spatial region. When $s = 4d$, the streamlines do not show any entrainment of the crossflow fluid, and roughly resemble the flow past a circular obstacle. The counter–rotating vortex pair (CVP) is clearly seen and seems to extend across the jet. In general, moving away from the jet–exit, the size of the CVP appears to increase. However, the jet appears slightly displaced from the CVP, particularly when $s > 4d$. The velocity contours indicate the jet to be above (+'ve n side) the CVP. This explains why the trajectory of a jet defined as the center streamline penetrates deeper into the crossflow than a trajectory defined based on the vorticity (Fearn & Weston 1974). Imagine the jet to carry a passive scalar. Due to the CVP being below the origin, and because the leading edge of the the jet is close to the origin, it might be guessed that comparatively more fluid containing the scalar would be seen below the origin ('-'ve n side) than above the origin. As mentioned earlier, the origin represents the point where the center streamline crosses the z–n plane. Hence, a trajectory based on the scalar centerline would penetrate less into the crossflow than the center streamline. Note that moving away from the jet–exit, the size of the jet cross–section and that of the CVP increases, which would suggest that the difference between the two trajectories increases with the distance from the jet–exit.

Figures 11(d)–(f) also show the horseshoe vortex close to the wall. These horseshoe vortices are formed upstream of the jet, similar to the ones formed around an obstacle in a boundary layer flow. They wrap around the jet and extend far into the downstream. The horseshoe vortices have been studied in detail, notably by Krothapalli *et al.* (1990) for a square jet in crossflow and by Kelso & Smits (1995) for a round jet in crossflow. Note that since the planes are not perpendicular to the wall, figures 11(d)–(f) do not show the true profile of the horseshoe vortex.

D. Jet trajectory

The trajectory of the jet has been the subject of considerable investigation. Models for jet trajectories have been suggested by Broadwell & Breidenthal (1984), Karagozian (1986), Hasselbrink & Mungal (2001) and Muppidi & Mahesh (2005). Broadwell & Breidenthal consider the jet–exit as a point source of momentum and, using similarity theory, conclude that the global length scale in this problem is 'rd'. The trajectory is scaled as

$$\frac{y}{rd} = A\left(\frac{x}{rd}\right)^B \tag{3}$$

where A and B are constants. Pratte & Baines (1967) obtain $A = 2.05$ and $B = 0.28$ from their experimental results. Margason (1993) provides a list of experimental values for A and B. Various experimental results in the literature provide a scatter in the value for these constants, $1.2 < A < 2.6$ and $0.28 < B < 0.34$. Muppidi & Mahesh (2005) show, by plotting trajectories from a few experiments on rd axes, that this rd scaling does not completely collapse trajectories and hence results in a considerable scatter (Muppidi & Mahesh (2005), figure 1). One reason for this lack of collapse is that the near–field of the jet-exit and jet trajectory depend not only on the velocity ratio r but also on the velocity profiles of the jet and of the crossflow. By performing controlled

simulations at two velocity ratios, two velocity profiles for the jet and by varying the crossflow boundary layer thickness, it was shown that rd scaling is insufficient to scale the trajectories (Muppidi & Mahesh (2005), figures 7 & 8). A scaling law was proposed which would take the velocity profile parameters into account, to scale the trajectory.

The jet trajectory was explained in terms of the competing inertias of the jet and of the crossflow. A near field parameter 'h' was defined as the height until which the jet remained vertical. Under the hypothesis that at h, the inertia of the jet was comparable to the pressure gradient applied by the crossflow on the jet (and hence to the momentum flux of the crossflow), the analytical equation relating h to the different parameters was presented as

$$\int_0^h d\left\{\frac{u_{cf}}{u_\infty}\right\}^2 \text{ dy } = C_m r^2 \pi \frac{d_j^2}{4}, \tag{4}$$

where h appears as the integral limit on the left hand side, u_{cf} is the crossflow velocity (and a function of y), and d_j is *effective diameter* of the jet defined as

$$\rho_j \int_A u_j^2 \text{ dA} = \frac{\pi d_j^2}{4} \rho_j \overline{u_j}^2 \tag{5}$$

where u_j on the left hand side is a function of the spatial coordinate (x, z in the present problem) and $\overline{u_j}$ is the mean jet velocity. Note that d_j allows the jet velocity profile to be parameterized. It was shown that equation 4 displayed the dependence of h on r and the jet and crossflow velocity profiles that was consistent with the observed results of the simulations. An analytical method to estimate h was presented by approximating the crossflow velocity u_{cf} as a piece–wise linear function of y :

$$\begin{aligned} \frac{h}{d} &= \left\{\frac{3}{4}\pi C_m r^2 \frac{\delta^2 d_j^2}{d^4}\right\}^{\frac{1}{3}}, \text{ when } h \le \delta, \text{ and} \\ \frac{h}{d} &= \frac{2}{3}\frac{\delta}{d} + \frac{\pi}{4} C_m r^2 \frac{d_j^2}{d^2}, \text{ when } h \ge \delta. \end{aligned} \tag{6}$$

and a scaling law

$$\frac{y}{rd} = A' \left(\frac{x}{rd}\right)^B \left(\frac{h}{d}\right)^C \tag{7}$$

was proposed, where C is 0.15 and A' and B are constants. Since equation 7 contains h, effects of velocity profiles of the jet and the crossflow, along with r, on the jet trajectory are taken into account. Figure 15 in Muppidi & Mahesh (2005) shows that scaling jet trajectories using equation 7 reduces the scatter significantly, thereby supporting the use of h to account for the effect of the jet and crossflow velocity profiles on the jet–trajectory. The scope of that study (Muppidi & Mahesh 2005) was confined to scaling the trajectories from the different simulations using h. A way to *predict* jet trajectories using h is now presented.

As mentioned previously, values of A found in the literature demonstrate a large scatter in the range of 1.2–2.6. An important reason ascribed to this scatter is the different definitions used to define the jet trajectory (Hasselbrink & Mungal 2001). Despite a complete consistency in this definition (the trajectory is defined as the center streamline on the symmetry plane), Muppidi & Mahesh (2005) obtain values of A ranging between 1.45 and 2.39 (see 1). B had a comparatively small range, $0.32 < B < 0.34$. A comparison of equations 3 and 7 shows that the constant A from the first equation is now substituted by the term $A'(h/d)^C$ in the second. Table 1 provides the values of A, h and A' from the nine simulations reported in Muppidi & Mahesh (2005). It maybe observed that the spread of A' is less than that seen in A, and more significantly, a majority of values for A' seem to lie around 1.8. An average value for A' obtained from table 1 is 1.85. In order to use equation 7 to predict the jet trajectory, an estimate for h is required. Using equation 6 and the parameters for the current simulation ($\delta = 1.32d$, $d_j = 1.05d$, $r = 5.7$), the estimated value for h is $2.29d$. Since h is defined as the height up to which the trajectory is vertical, this value can also be extracted as the y coordinate of the trajectory at a small distance downstream of the jet–exit. The value of h thus extracted (as the y coordinate at $x = 0.05$ d) from the trajectory provides $h = 2.62$ d, a difference of about 11%. Approximating the crossflow velocity profile with the piece–wise linear function might be a reason for this discrepancy. Thus, having computed h, and taking the

	h	A	A'
1	0.608268	2.0215	2.1780
2	0.528857	1.75505	1.9310
3	0.323492	1.58726	1.8800
4	0.255544	1.45267	1.7826
5	2.573220	2.13378	1.8517
6	2.375180	1.99401	1.7513
7	1.844540	2.00177	1.8261
8	1.764860	1.86196	1.7099
9	3.145660	2.39052	2.0129

Table 1. Values of near–field scaling parameter h, and the constants A and A', from the simulations in Muppidi & Mahesh (2005).

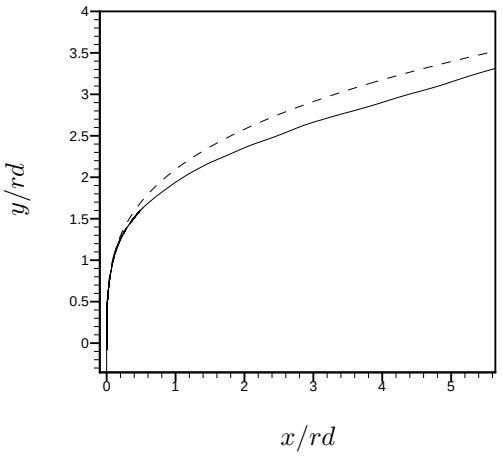

Figure 10. Jet trajectory predicted using equation 7 (– – – –) compared to the jet trajectory obtained from the simulation (———).

value of A' as 1.85, the jet trajectory can be predicted. Figure 10 shows the predicted trajectory along with the trajectory obtained from the simulations. Note that the agreement is reasonable. Even as far away as $4rd$ (about 23 diameters downstream of the jet–exit) downstream of the jet–exit, the difference between the predicted and the actual trajectories is about 9%, which appears reasonable.

V. Summary

Direct numerical simulations of a round turbulent jet in crossflow are performed. The conditions are the same as the experiments of Su & Mungal (2004). Velocity and turbulent intensity profiles from the simulation are compared to those from the experiments. It is seen that the profiles, when scaled with the velocity ratio r do not completely agree. The cause of the discrepancy is shown to be the jet–to–crossflow density ratio in the experiments, and this factor explains the differences seen. The profiles are re–scaled with the 'effective velocity ratio' r_{eff} and it is shown that such re–scaling brings the profiles and the jet–trajectory from the simulations closer to the experimental results and the agreement observed is good. The different stages seen as the jet evolves from one of a circular cross–section in the near–field to a 'kidney–shaped' structure in the far field are presented. The evolution of the CVP along the length of the jet is also studied. The CVP forms very close to the jet–exit on the downstream edge of the jet. Moving away from the jet–exit, the CVP appears to increase in size. A

study of this evolution also explains why a jet trajectory based on the center streamline penetrates deeper than one defined based on either the vorticity or the scalar concentration. The jet trajectory is predicted using the scaling law proposed by Muppidi & Mahesh (2005) and the prediction is shown to be satisfactory. Scaling and predicting jet trajectories in this manner aids in accounting for different jet and crossflow velocity profiles that the existing rd scaling cannot.

Acknowledgments

This work was supported by the National Science Foundation under grant CTS–0133837. Computer time was provided by The National Center for Supercomputing Applications (NCSA), Minnesota Supercomputing Institute (MSI) and the San Diego Supercomputer Center (SDSC).

References

[1]Andreopoulos, J. & Rodi, W. 1984 Experimental investigation of jets in a crossflow *J. Fluid Mech.* **138:** 93–127.

[2]Broadwell, J.E. & Breidenthal, R.E. 1984 Structure and mixing of a transverse jet in incompressible flow *J. Fluid Mech.* **148:** 405–412.

[3]Chochua, G., Shyy, W., Thakur, S., Brankovic, A., Lienau, K., Porter, L. & Lischinsky, D. 2000 A computational and experimental investigation of turbulent jet and crossflow interaction. *Numer. Heat Transfer, Part A.* **38:** 557–572.

[4]Eggels, J.G.M., Unger, F., Weiss, M.H., Westerweel, J., Adrian, R.J., Friedrich, R. & Nieuwstadt, T.M. 1994 Fully developed turbulent pipe flow : a comparison between numerical simulation and experiemnt. *J. Fluid Mech.* **268:** 175 –209.

[5]Fearn, R.L. & Weston, R.P. 1974 Vorticity associated with a jet in crossflow. *AIAA J.* **12:** 1666–1671.

[6]Fric, T.F. & Roshko, A. 1994 Vortical structure in the wake of a transverse jet *J, Fluid Mech.* **279:** 1–47.

[7]Hasselbrink, E.F & Mungal, M.G. 2001 Transverse jets and jet flames. Part 2. Velocity and OH field imaging *J. Fluid Mech.* **443:** 27–68.

[8]Karagozian, A.R. 1986a An analytical model for the vorticity associated with a transverse jet *AIAA J.* **24:** 429–436.

[9]Kamotani,Y. & Greber, I. 1972 Experiments on turbulent jet in a crossflow *AIAA J.* **10:** 1425 – 1429.

[10]Keffer, J.F. & Baines, W.D. 1963 The round turbulent jet in a cross wind *J. Fluid Mech.* **15:** 481–496.

[11]Kelso, R.M. & Smits, A.J. 1995 Horseshoe vortex systems resulting from the interaction between a laminar boundary layer and a transverse jet *Phys. Fluids* **7:** 153–158.

[12]Kelso, R.M., Lim, T.T & Perry, A.E. 1996 An experimental study of round jets in cross–flow. *J. Fluid Mech.* **306:** 111–144.

[13]Krothapalli, A., Lourenco,L. & Buchlin, J.M. 1990 Separated flow upstream of a jet in a crossflow *AIAA J.* **28:** 414–420.

[14]Mahesh, K., Constantinescu, G. & Moin, P. 2004 A numerical method for large–eddy simulation in complex geometries. *J. Comput. Phys.* **197:** 215–240.

[15]Margason, R.J. 1993 Fifty years of jet in crossflow research. In *AGARD Symp. on a jet in Cross Flow, Winchester, UK, AGARD CP*–534.

[16]Muppidi, S. & Mahesh, K. 2005 'Study of trajectories of jets in crossflow using direct numerical simulations' *J. Fluid. Mech.*, accepted for publication.

[17]Pratte, B.D. & Baines, W.D. 1967 Profiles of the round turbulent jet in a cross flow *J. Hydraul. Div., ASCE* **92** (HY6), 53–64.

[18]Schlichting, H.T. 1963 Boundary Layer Theory, McGraw Hill.

[19]Schluter, J.U. & Schonfeld, T. 2000 LES of Jets in Crossflow and its Application to a Gas Turbine Burner *Flow Turbulence and Combustion* **65(2):** 177–203.

[20]Shan, J.W. & Dimotakis, P.E. 2001 Turbulent mixing in transverse jets *GALCIT FM:2001.006.*

[21]Sherif, S.A. and Pletcher, R.H. 1989 Measurements of the Thermal Characteristics of Heated Turbulent Jets in Cross Flow. *ASME J. Heat Transfer* **111:** 897–903.

[22]Smith, S.H. & Mungal, M.G. 1998 Mixing, structure and scaling of the jet in crossflow *J. Fluid Mech.* **357:** 83–122.

[23]Su, L.K. & Mungal, M.G. 2004 Simultaneous Measurement of Scalar and Velocity Field Evolution in Turbulent Crossflowing Jets *J. Fluid Mech.* **513:** 1–45.

[24]Yuan, L.L. & Street, R.L. 1998 Trajectory and entrainment of a round jet in crossflow *Phys. Fluids* **10:** 2323–2335.

[25]Yuan, L.L., Street, R.L. & Ferziger, J.H. 1999 Large–eddy simulations of a round jet in crossflow *J. Fluid Mech.* **379:** 71–104.

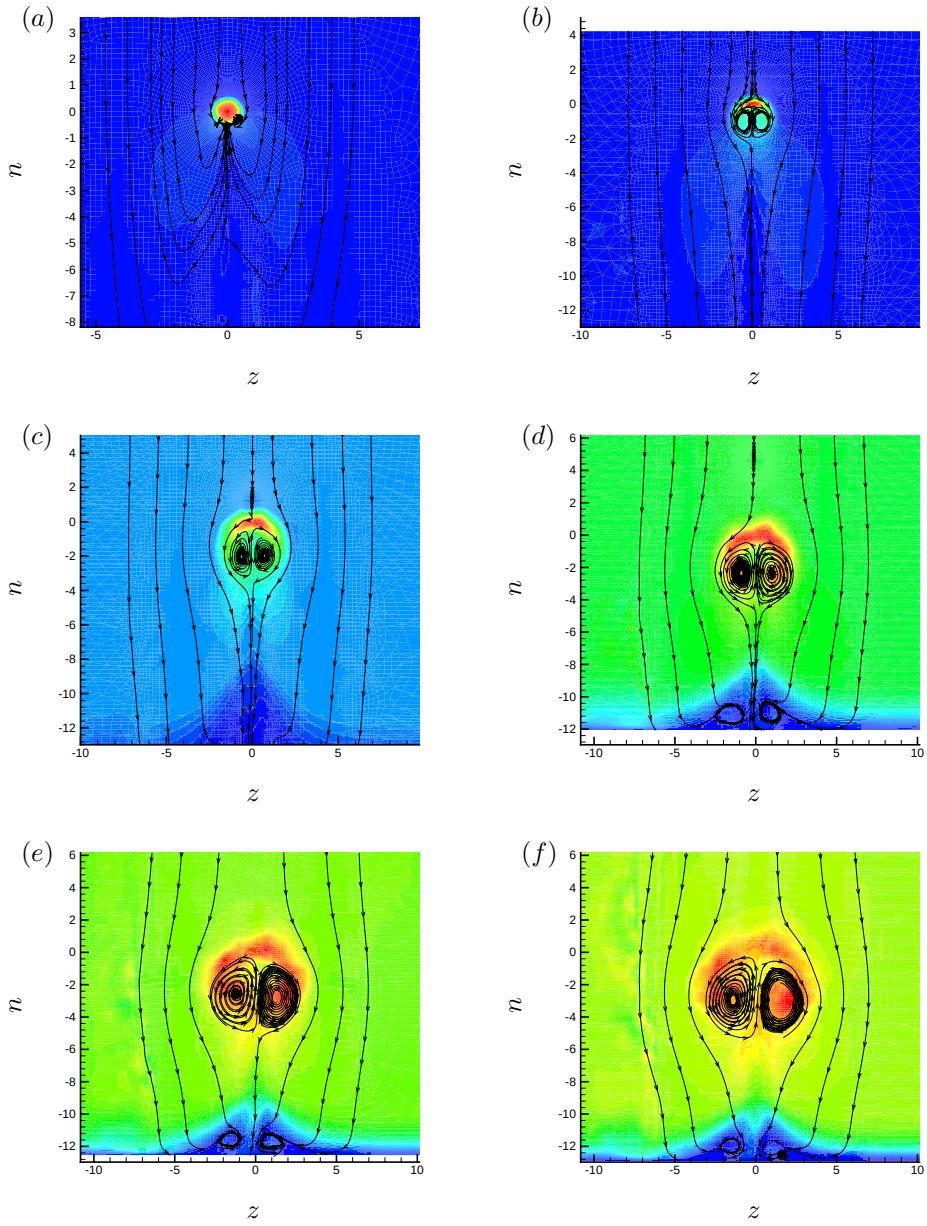

Figure 11. Evolution of the jet at different points along the jet centerline. Shown are contours of out–of–plane velocity and on planes normal to the jet. The location of the jet is (a) $s = d$, (b) $s = \mathbf{4}d$, (c) $s = \mathbf{7}d$, (d) $s = \mathbf{10}d$, (e) $s = \mathbf{13}d$ **and** (f) $s = \mathbf{15}d$.